engineering proceedings

MDPI

*Proceeding Paper*

# 3D Printable Piezoelectric Composite Sensors for Guided Ultrasonic Wave Detection †

**Thomas Roloff *, Rytis Mitkus, Jann Niklas Lion and Michael Sinapius**

Institute of Mechanics and Adaptronics, Technische Universität Braunschweig, 38106 Braunschweig, Germany; r.mitkus@tu-braunschweig.de (R.M.); j.lion@tu-braunschweig.de (J.N.L.); m.sinapius@tu-braunschweig.de (M.S.)

* Correspondence: thomas.roloff@tu-braunschweig.de; Tel.: +49-531-8069

† Presented at the 8th Electronic Conference on Sensors and Applications, 1–15 November 2021; Available online: https://ecsa-8.sciforum.net/.

**Abstract:** Commercially available photopolymer resin is combined with Lead Zirconate Titanate (PZT) micrometer size piezoelectric particles to form 3D printable suspensions that solidify under UV light. This in turn allows achieving various non-standard sensor geometries that might bring benefits, such as increased piezoelectric output in specific conditions. However, it is unclear whether piezoelectric composite materials are suitable for Guided Ultrasonic Wave (GUW) detection, which is crucial for Structural Health Monitoring (SHM) in different applications. In this study, thin piezoelectric composite sensors are tape casted, solidified under UV light, covered with electrodes, polarized in a high electric field and adhesively bonded onto a wave guide. This approach helps to understand the capabilities of thin piezoelectric composite sensors for GUW detection. In an experimental study, thin 2-dimensional rectangular, circular and annulus segment shaped piezoelectric composite sensors with an effective surface area smaller than 400 $mm^2$ applied to an aluminum plate with a thickness of 2 mm demonstrate successful detection of GUW up to 250 kHz. An analytical calculation of the maximum and minimum amplitude for the ratio of the wavelength and the sensor length in wave propagation direction shows good agreement with the sensor-recorded amplitude. The output of the piezoelectric composite sensors is compared to commercial piezoelectric discs to evaluate their performance.

**Keywords:** piezocomposite sensor; structural health monitoring; guided ultrasonic waves; sensor geometry



**Citation:** Roloff, T.; Mitkus, R.; Lion, J.N.; Sinapius, M. 3D Printable Piezoelectric Composite Sensors for Guided Ultrasonic Wave Detection. *Eng. Proc.* **2021**, *10*, 36. https://doi.org/10.3390/ecsa-8-11308

Academic Editor: Stefano Mariani

Published: 1 November 2021



## 1. Introduction

In the emerging field of Structural Health Monitoring (SHM) for large plate-like and complex thin-wall structures, Guided Ultrasonic Waves (GUW) are a state of the research to detect damages and evaluate the condition of the structure. GUW interfere with structural changes, e.g., stringers, which leads to a complex wave field. To guarantee reliable measurements, direction sensitive actuation and sensing is under investigation [1]. Direction sensitivity is closely connected to the sensor size and dimensions [2] (p. 359ff). Therefore, the idea is that the shape of the sensor has an influence on the GUW detection, too. Manufacturing methods, such as 3D printing or tape casting, allow almost free-form design of piezoelectric composite sensors that are solidified with UV light from suspensions made of PZT particles dispersed in a photopolymer resin. Application-specific free-form designed, variable-, direction- and mode-sensitive sensors could lead to a major extension of existing SHM setups.

GUW are dispersive waves that appear in structures with two parallel free surfaces. They occur in symmetric and asymmetric modes and show displacements inside and on the surface of a structure. The particles perform in-plane and out-of-plane movements [3] and [4] (p. 198ff). GUW are well suited for SHM applications due to their low damping over long distances [5] (p. 6).

Solid piezoceramic discs are state of the art for GUW detection [4] (p. 239ff.), but other piezoelectric materials exist, e.g., piezoelectric polymers or piezocomposite materials. Pure piezoceramics are stiff and brittle, cannot be applied on curved surfaces and often cause high reflections of GUW due to their high acoustic impedance [6]. Piezoelectric photopolymers, such as polyvinylidene fluoride (PVDF), are very flexible but offer a low electromechanic coupling and sensitivity. The aim of piezoelectric composite materials is to combine the advantages of both.

One of the first mentions of piezoelectric composites in the field of SHM applications in the literature was Giurgiutiu and Lin in 2004 [7] with the in situ fabrication of piezoelectric wafer active sensors (PWAS) using a piezoelectric composite approach. Additive manufacturing methods of flexible piezoelectric composites are rarely mentioned in the SHM field. Investigations on 3D printed piezoelectric composites are undertaken but mostly in other subject fields (e.g., energy harvesting and ultrasonic or biomedical imaging) [8,9]. In most cases, the piezoelectric material PZT is used because of the very high piezoelectric properties compared to most piezoelectric materials ($d_{33,PZT} = 225 - 590\,\mathrm{pC\,N^{-1}}$) [10]. In particular, polymer- [11,12] and cement-based matrices [13] are used as the inactive phase of the composite.

However, the effect of the sensor geometry was not investigated, but modifications are possible just as mode-selective and directive actuators and sensors, e.g., sensor setups with interdigital electrodes [1]. The mode-selectivity and directivity is strongly connected to the sensor geometry [2] (p. 359ff). This fact will be described briefly in the following paragraph to give the basics for the evaluation in Section 3.

When idealized as a plate capacitor, the generated voltage by a rectangular piezoelectric sensor under mechanical deformation can be calculated as follows:

$$U = \frac{d_{31} t_s Y_s}{\varepsilon_{33}^{\sigma} 2a2b(1-\nu)} \iint_A (\varepsilon_x + \varepsilon_y)\, dx\, dy \tag{1}$$

where $d_{31}$ denotes the piezoelectric charge coefficient, $t_s$ the sensor thickness, $2a$ the sensor length, $2b$ the sensor width, $Y_s$ the Young's modulus of the sensor, $\varepsilon_{33}^{\sigma}$ the dielectric constant at constant mechanical stress, $\nu$ the Poisson's ratio and $\varepsilon_x$ and $\varepsilon_y$ the strains on the surface of the structure [14].

In the following consideration, a planar, one-dimensional Lamb wave field is assumed, generating strain in the $x$-direction on the plate surface. All parameters except the sensor length are kept, and the sensor is assumed to be a 1D piezoelectric resonator. Then the first amplitude maximum and minimum for the different modes occur at the following wavelengths $\lambda$, with a detailed description in [1] (p. 21f) and [4] (p. 249ff):

$$\text{First sensor amplitude maximum at: } \lambda = 4a, \tag{2}$$

$$\text{First sensor amplitude minimum at: } \lambda = 2a. \tag{3}$$

The previous statements show that the sensor performance (i.e., maximum voltage generated) depends on multiple parameters with size and geometry playing a key role.

This study experimentally investigates the applicability of 3D printable piezoelectric composite sensors for GUW detection. In addition, the first insight into the geometry dependency of the signal generation under GUW excitation is provided. GUW detection in an isotropic medium up to a frequency–thickness ratio of at least $fd = 0.5\,\mathrm{MHz\,mm}$ is validated, which makes these sensors applicable for SHM setups. The results give the appearance that the geometry of the sensor and sensor orientation with respect to the wave propagation direction play a key role in the sensor behavior. This behavior will be subject to future research.

## 2. Materials and Methods

The suspensions used to manufacture sensors throughout this study consist of 20 vol% PZT particles (material: PIC255, average particle size 1.6 µm, PI Ceramic, Lederhose,

Germany) dispersed randomly in a photopolymer resin (High Temperature resin V2, Formlabs, Somerville, MA, USA) with a centrifugal mixer (Speedmixer DAC 700.2 VAC-P, Hauschild GmbH & Co. KG, Hamm, Germany). Materials are selected based on our previous studies [15,16]. No solvents or any other additives are used in suspension preparation. To achieve proper dispersion of the particles, the suspension is mixed under vacuum (20 mbar) three times with the following parameters: 1 min at 900 $min^{-1}$, 0.5 min at 1250 $min^{-1}$ and 4 min at 1750 $min^{-1}$. The dispersion quality is proven with Scanning Electron Microscopy (SEM) imaging. Figure 1 shows an SEM image of the piezocomposite at a magnification factor of 10,000×. The cured photopolymer appears darker, and the embedded PZT particles are brighter. No agglomerations occur, and the particle distribution can be assumed as homogeneous. Because of the high density of PZT particles compared to the photopolymer ($\rho_{PZT} = 7.85\,g\,cm^{-3}$, $\rho_{photopolymer} = 1.14\,g\,cm^{-3}$), the suspension sediments in 24 h. Therefore, the suspension is remixed each time before sensor manufacturing.

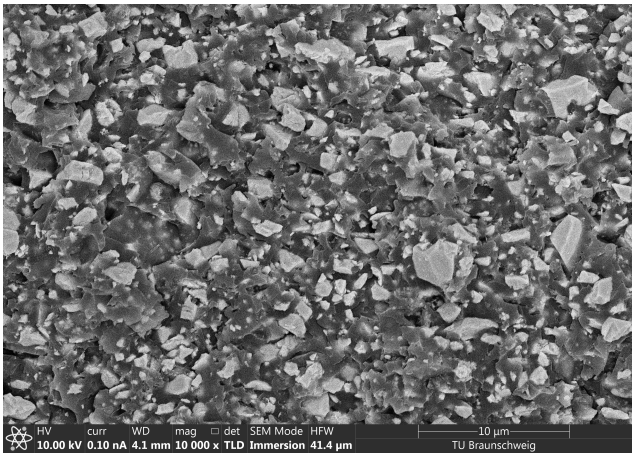


**Figure 1.** Scanning Electron Microscopy image of 20 vol% PZT/photopolymer composite shows homogeneous particle dispersion and no agglomerations

### *2.1. Sensor Manufacturing*

The sensors are manufactured by tape casting. A PVC foil sticker (Oraguard 270G, thickness 150 µm, ORAFOL GmbH, Oranienburg, Germany), with the required sensor geometry pre-cut by a plotter, is glued on glass. The suspension is filled on the sticker and tape casted manually with a metal blade held at 30° from vertical position. The glass with tape casted sensors is placed 50 mm below a UV light source (EQ CL30 LED Flood 405, Loctite/Henkel AG, Düsseldorf, Germany) for 60 s for solidification.

Five individual measurements along the sensor surface are used to determine the respective sensor thicknesses required for dielectric measurements and polarization. Another pre-cut PVC sticker with electrode geometry (1 mm offset from outer edges of the sensor) is adhered onto the sensor. Silver-coated copper (843AR Super Shield Silver Coated Copper Conductive Coating, MG Chemicals, Ontario, Canada) is sprayed manually in two thin layers as an electrode. After drying, the sticker is peeled off, leaving the electrode on the sensor, and the same procedure is repeated on the other side.

To polarize the sensors, a 55 kV $mm^{-1}$ DC electric field is applied for 21 min in total (4 min ramp up, 16 min hold, 1 min ramp down) in a warm silicone oil at 65 °C. After polarization, the sensors are dried with a paper towel and are left for a minimum of 24 h to dry further. Conductive silver ink (Silber-Leitlack, Busch GmbH & Co. KG, Viernheim, Germany) is used on the corner of each sensor to generate single-side access to both electrodes and ensure full and even sensor adhesion to the aluminum wave guide.

Table 1 presents the mechanical, dielectric and piezoelectric properties of both piezocomposite and commercial piezoelectric sensor (PRYY-1126, material: PIC255, diameter 16 mm, ceramic height: 200 µm, PI Ceramic GmbH, Lederhose, Germany) material. Their

calculation and measurements are presented in detail in our previous publication [16]. Young's modulus is measured using tensile testing adapted to thin film testing. The electromechanical coupling factor $k_{31}$ is calculated as follows

$$k_{31} = \sqrt{\frac{d_{31}^2}{s_{11}^E \varepsilon_{33}^T}}, \quad (4)$$

where $s_{11}^E$ denotes the elastic compliance at no electric field (inverse of Young's modulus) and $\varepsilon_{33}^T$ the dielectric constant at no mechanical stress.

**Table 1.** Properties of the piezoelectric materials under investigation.

| Material | Young's Modulus (Perp. to Pol. Dir.) $Y$ (GPa) | Dielectric Permittivity at 1 kHz $\varepsilon_{33}$ (nF m$^{-1}$) | Piezoelectric Charge Constant $d_{31}$ (pC N$^{-1}$) | Electromechanical Coupling Factor $k_{31}$ (-) |
|---|---|---|---|---|
| Piezocomposite | $1.8 \pm 0.2$ | $0.08 \pm 0.002$ | $-0.92 \pm 0.13$ | $0.0044 \pm 0.00091$ |
| Commercial ceramic (PIC255) [6] | 62.1 | 15.1 | $-180$ | 0.35 |

### 2.2. Sensor Geometry Selection

For comparability, the sensor's electrode surfaces are set to 324 mm$^2$. The overall size of the sensors with different geometries may vary due to the 1 mm offset. The mean sensor thickness is 129.9 µm, and the average electrode thickness is 44.3 µm. In addition to conventional geometries (square and circle), the more complex geometry of an annulus segment is investigated. Its radii are adapted to the expected propagating wavefront of a circular actuator. Figure 2 shows the respective sensor geometries and a commercial circular piezoceramic sensor in respective orientation to the wave propagation direction.

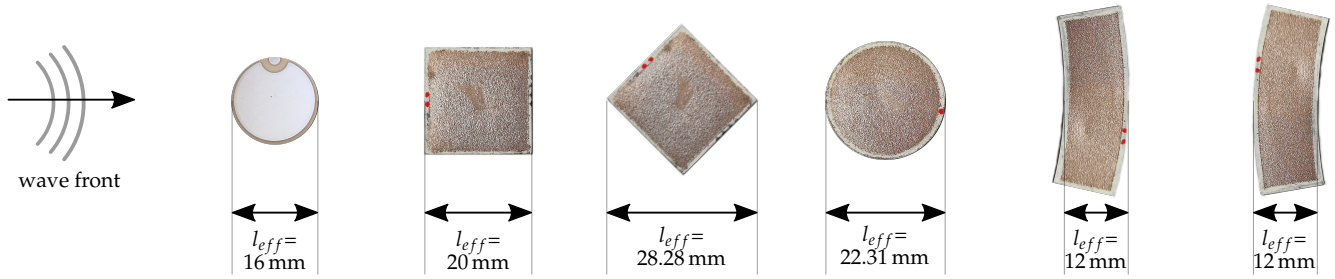


**Figure 2.** Sensor shapes under investigation with regard to the wave propagation direction and assumptions concerning the effective sensor length in wave propagation direction. (**a**) Wave front of a circular wave field. (**b**) Commercial Piezoceramic PRYY-1126. (**c**) Sensor shape: square (Orientation: 1). (**d**) Sensor shape: square (Orientation: 2). (**e**) Sensor shape: circle (Orientation: -). (**f**) Sensor shape: annulus seg. (Orientation: 1). (**g**) Sensor shape: annulus seg. (Orientation: 2).

### 2.3. Determination of Detectable GUW Signals

The test setup is shown in Figure 3. A square aluminum plate (material 3.3535) with an area of 1 m × 1 m and a thickness of 2 mm is used as a wave guide. A piezoceramic disc actuator PRYY-1126 is used for excitation and adhesively bonded to the center of the plate with cyanoacrylate. Due to the circular ceramic, the wave field is assumed to have a concentrically propagating circular wave front. The sensors are equally glued to the aluminum plate in a circular arrangement with the sensors geometric center on a circle with a radius of 156 mm around the actuator. The sensors under investigation will be placed in two orientations with respect to the wavefront except for the circular ones—see Figure 2. A PicoScope 5442B is used in combination with a laptop to serve as a signal generator to provide the excitation signal, and the amplification is realized using a high voltage

amplifier WMA-300 (Falco Systems, Katwijk aan Zee, The Netherlands). The laptop with the PicoScope also acquires the measurement data.

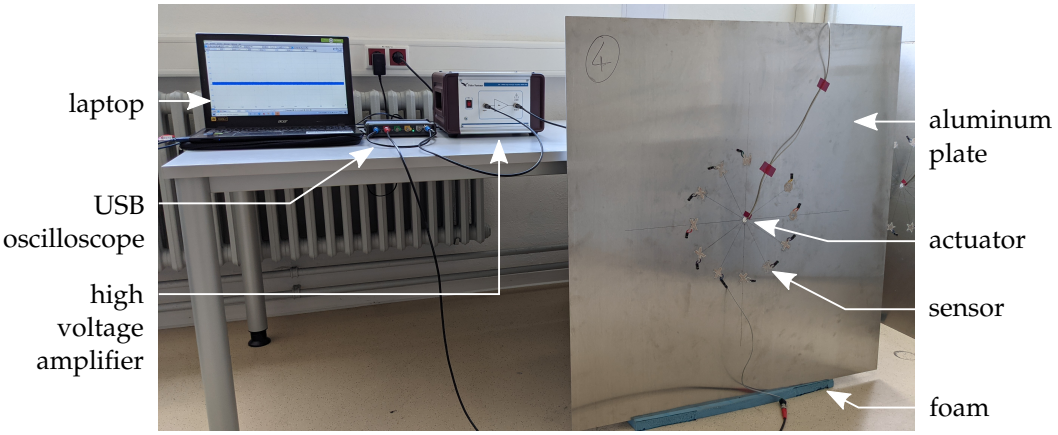


**Figure 3.** Test setup to determine the peak-to-peak voltage of the sensors under GUW excitation.

For excitation, a 5-cycle, hanning-windowed sine burst is used. The investigated burst center frequencies range from 5 kHz to 200 kHz with an interval of 5 kHz and from 200 kHz to 250 kHz with an interval of 25 kHz. Due to the short distance between the actuator and the sensors, no temporal separation of the $S_0$ and $A_0$ modes is possible. Therefore, the peak-to-peak voltage amplitude $U_{pp}$ is measured in a time window from the calculated start of the faster $S_0$ to the end of the slower $A_0$ mode—see Figure 4. To generate comparable sensor signals, a normalization is performed. The signals are normalized using the sensor's thicknesses, a factor to compensate the capacity loss due to polarization errors and a factor to compensate for the amplifier behaviour, as the amplification factor decreases with increasing frequency depending on the capacitive load.

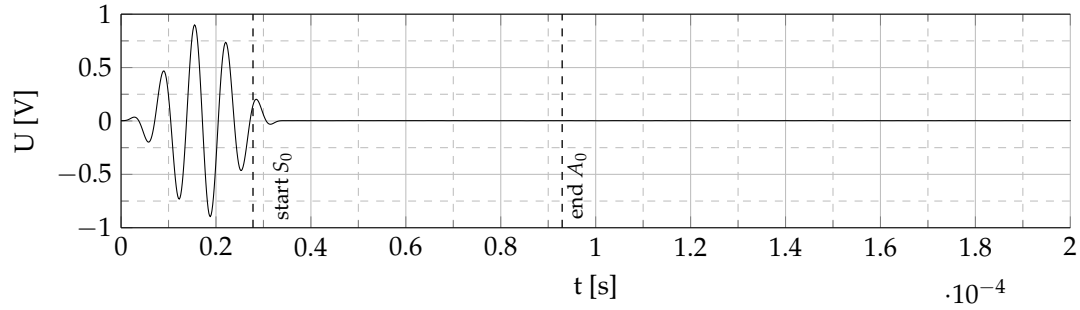


(**a**)

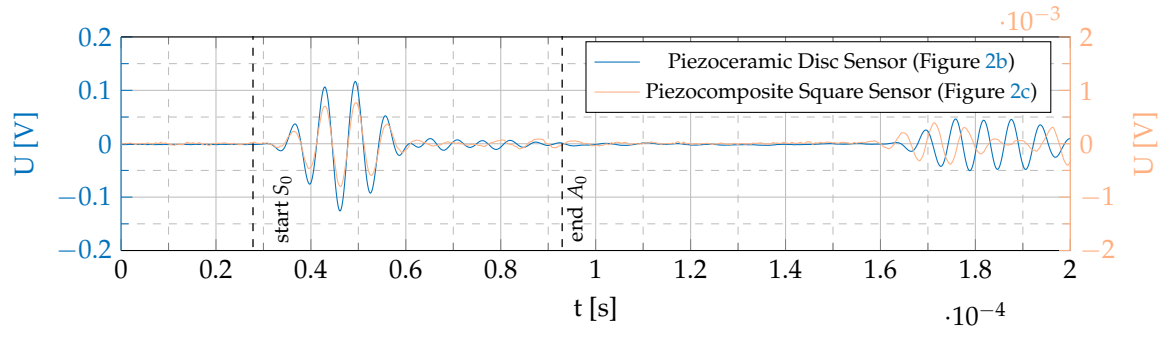


(**b**)

**Figure 4.** Exemplary signal comparison of a commercial piezoelectric disc sensor and a piezocomposite square sensor under GUW excitation. Dashed lines indicate the estimated start and end times of the faster $S_0$ and slower $A_0$ wave package, respectively, at the sensor location. (**a**) Excitation signal before amplification: 5-cycle hanning-windowed sine burst with a burst center frequency of $f_c = 150$ kHz. (**b**) Sensor signals.

## 3. Results and Discussion

The overall aim of this study is to show that 3D printable piezocomposite sensors are capable of detecting GUW. Figure 4 shows an exemplary time signal of the generated voltage $U$ by a piezocomposite sensor in comparison with a commercial piezoelectric disc sensor. These data were generated using the setup described in Section 2.3. Although the generated voltage by the piezocomposite sensor is two powers of ten lower, it shows the same qualitative behavior as the commercial one. This leads to the conclusion that the presented 3D printable piezocomposite sensors are capable of detecting GUW and might be suitable to be used in SHM setups. The higher amplitude of the piezoceramic sensor is due to a higher thickness ($h_{PRYY-1126} = 200\,\mu m$, $h_{piezocomposite} = 129.9\,\mu m$), stiffness and piezoelectric charge coefficient (see Equation (1) and Table 1). The coefficient of the commercial PRYY-1126 sensor is approx. 200 times higher than the one of the piezocomposite sensor.

Apart from the general proof that the piezocomposite sensors are capable of detecting GUW, the first insight into the frequency and geometry dependency of the generated voltage is presented in the following paragraphs. The results for the sensors shown in Figure 2, manufactured and measured as described in Section 2, are presented in Figure 5.

All sensors show a qualitatively similar behavior with maxima and minima at different frequencies, as expected in Section 1. According to Equations (2) and (3) and the assumption of a 1D wave propagation, the expected frequencies/wavelengths for a maximum or minimum amplitude for a given sensor length are calculated and shown as solid and dotted vertical lines, respectively. Figure 2 shows the assumed effective sensor lengths in the wave propagation direction. The frequency-dependent wavelengths of the wave guide are calculated using the *Dispersion Calculator* developed at the *German Aerospace Center* (DLR). The analytical results for the expected maximum and minimum amplitudes fit well with the measurements of the annulus segment-shaped sensor and the square-shaped one in orientation 1. The two circular sensors show slight deviations from the calculated extrema, and the results of the rotated square sensor (orientation 2) deviate most from the analytical calculations. Possible explanations are erroneous material properties in the analytical solution, a superposition of the $A_0$ and $S_0$ mode as the group velocities do not differ enough for wave package separation and most likely a wrong estimation of the effective sensor length and an erroneous assumption of a 1D wave field.

Although the qualitative behavior is the same, the amplitudes differ between the different sensors. The commercially available piezoceramic sensor shows higher amplitudes than the custom piezocomposite sensors over the whole investigated frequency range. This phenomenon is already explained above. Furthermore, the maxima of the annulus segment-shaped sensor are higher than for the standard geometries (circular and square shape). This might give the impression that a short effective sensor length leads to higher amplitudes. This is only valid for a constant sensor width (see Equation (1)), and furthermore, the square-shaped sensor shows higher amplitudes for orientation 2 with a higher effective sensor length than for orientation 1. Moreover, the two measurements for the square sensor in orientation 2 differ considerably from one another. This shows that more profound investigations are necessary to reliably characterize these sensors.

Another interesting finding is that the annulus segment-shaped sensor shows better performance in orientation 2, although this is the one that is not adopted to the expected wave field.

Two possible explanations for the slight differences in the amplitudes between all of the piezocomposite sensors are to be discussed in further research: Firstly, the adapted radii of the annulus segment-shaped sensor to the expected wave field might lead to a higher instantaneous reflection of the incoming wave. This would result in a reduced vibration amplitude inside the sensor. Secondly, the emitted wave field from the actuator might not be concentric. It is a ceramic with a wrap-around contact that allows single-side access to the electrodes but results in an non-circular electrode surface on the top. Moreover, the resonance behavior of a piezoelectric actuator disc results in an inhomogeneous wave field

emission as well [17]. If the wave field is not concentric, the sensors undergo different excitations in their circular setup.

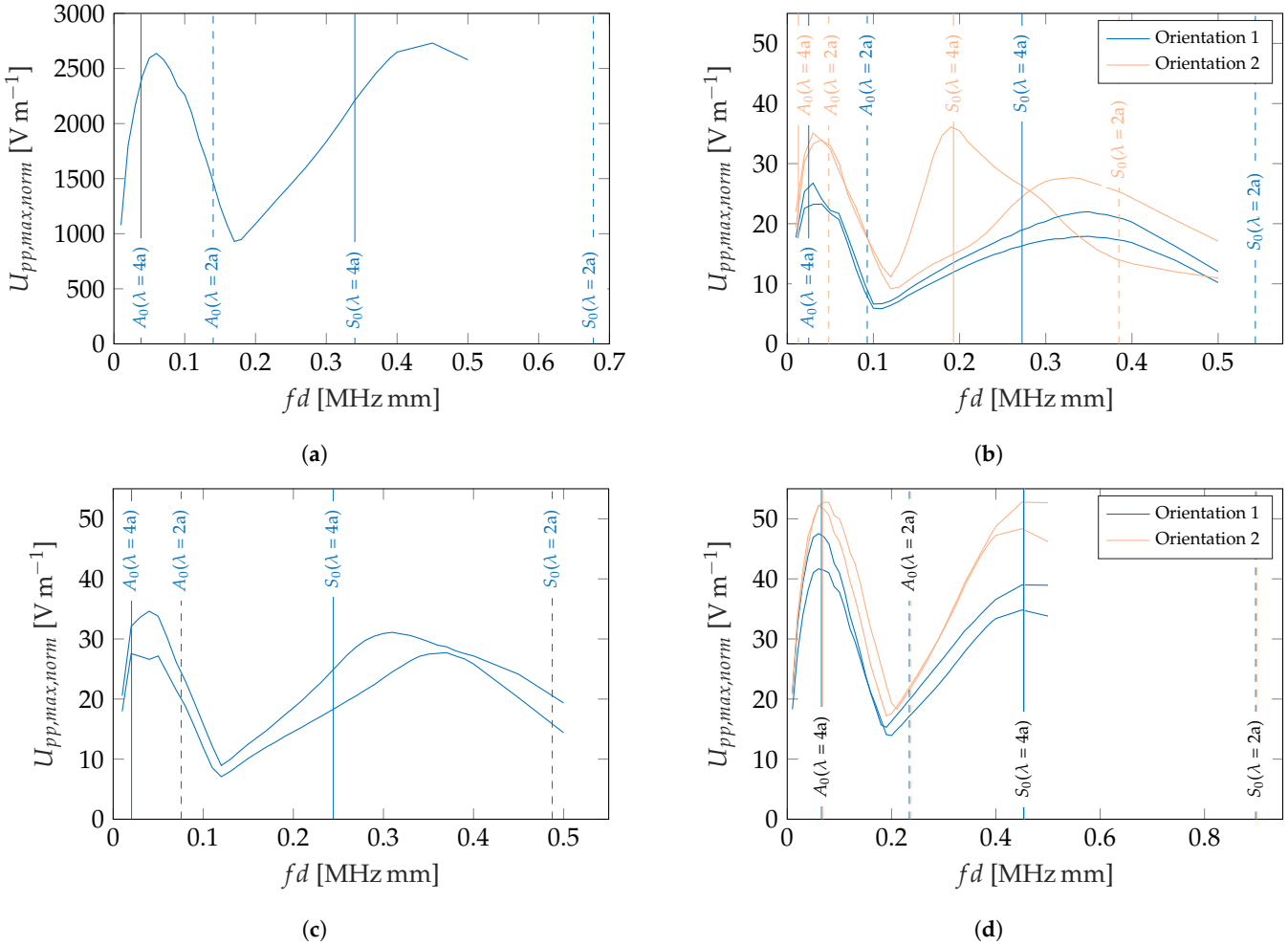


**Figure 5.** Experimentally determined peak-to-peak voltage for different sensor types, shapes and orientations under GUW excitation in a 2 mm aluminum plate, analytically calculated amplitude maxima (solid vertical lines) and minima (dotted vertical lines) based on estimated effective sensor lengths in wave propagation direction (see Figure 2, Equations (2) and (3)). (**a**) Commercial solid piezoceramic sensor, Figure 2b. (**b**) Piezocomposite sensor: square, Figure 2c,d. (**c**) Piezocomposite sensor: circle, Figure 2e. (**d**) Piezocomposite sensor: annulus segment, Figure 2f,g.

## 4. Conclusions

In this study, the detection of GUW in isotropic wave guides using tape-casted piezoceramic composite sensors based on photopolymers is validated. This is experimentally shown for an isotropic aluminum plate with 2 mm thickness for frequencies of up to at least 250 kHz. A rudimental setup revealed that different piezocomposite sensor sizes and shapes show different sensitivities and that their sensitivity can not reach the one of solid PZT discs yet. The geometry dependency is promising for future design of optimized piezocomposite GUW sensors.

To answer the open questions concerning the geometry dependency and to reach new forms of sensors, the following research topics have to be addressed in future publications:

- Optimize the material properties to increase the piezoelectric sensitivity;
- Consider geometry rather than only the estimated effective sensor length as a criterion, providing an analytical model to link the sensor response to an excited GUW wave field, e.g., a 3D linear elasticity model as presented in [18];

- Realizing a defined characterization environment to extract the sensor behavior in a sort of frequency response function that is independent from the sensor's excitation;
- Design a concept for variable, direction-sensitive and mode-selective sensors.

**Author Contributions:** Conceptualization, T.R., R.M., J.N.L. and M.S.; methodology, T.R., R.M. and J.N.L.; software, T.R., R.M. and J.N.L.; validation, T.R., R.M. and J.N.L.; formal analysis, T.R., R.M. and J.N.L.; investigation, T.R., R.M. and J.N.L.; resources, M.S.; data curation, T.R., R.M. and J.N.L.; writing—original draft preparation, T.R., R.M. and J.N.L.; writing—review and editing, T.R. and M.S.; visualization, T.R., R.M. and J.N.L.; supervision, M.S.; project administration, M.S.; funding acquisition, M.S. All authors have read and agreed to the published version of the manuscript.

**Funding:** The authors expressly acknowledge the financial support of the research work on this article within the Research Unit 3022 "Ultrasonic Monitoring of Fibre Metal Laminates Using Integrated Sensors" (Project number: 418311604) and the Research Project "Piezoelectric 0-0-3 Composites" (Project number: 389409970) by the German Research Foundation (Deutsche Forschungsgemeinschaft (DFG)).

**Institutional Review Board Statement:** Not applicable.

**Informed Consent Statement:** Not applicable.

**Data Availability Statement:** The raw data of the experiments can be requested from the authors.

**Conflicts of Interest:** The authors declare no conflict of interest. The funders had no role in the design of the study; in the collection, analyses, or interpretation of data; in the writing of the manuscript; or in the decision to publish the results.

## References

1. Schmidt, D. Modenselektive Übertragung von Lambwellen in Faserverbundstrukturen. Ph.D. Thesis, Technische Universität Braunschweig, Braunschweig, Germany, 2014.
2. Rose, J.L. *Ultrasonic Guided Waves in Solid Media*; Cambridge University Press: Cambridge, UK, 2014. [CrossRef]
3. Lamb, H. On waves in an elastic plate. *Proc. R. Soc. Lond.* **1917**, *93*, 114–128. [CrossRef]
4. Giurgiutiu, V. *Structural Health Monitoring with Piezoelectric Wafer Active Sensors*; Academic Press/Elsevier: Amsterdam, The Netherlands, 2008.
5. Lammering, R.; Gabbert, U.; Sinapius, M.; Schuster, T.; Wierach, P. (Eds.) *Lamb-Wave Based Structural Health Monitoring in Polymer Composites*; Springer eBook Collection; Springer: Cham, Switzerland, 2018. [CrossRef]
6. PI Ceramic GmbH. Datasheet—Material Data of Piezoelectric Materials: Specific Parameters of the Standard Materials. Available online: https://www.piceramic.de/fileadmin/user_upload/physik_instrumente/files/datasheets/PI_Ceramic_Material_Data.pdf (accessed on 17 December 2021).
7. Giurgiutiu, V.; Lin, B. In-Situ Fabrication of Composite Piezoelectric Wafer Active Sensors for Structural Health Monitoring. In Proceedings of the ASME 2004 International Mechanical Engineering Congress and Exposition, Anaheim, CA, USA, 13–19 November 2004; pp. 89–95. [CrossRef]
8. Chen, Z.; Song, X.; Lei, L.; Chen, X.; Fei, C.; Chiu, C.T.; Qian, X.; Ma, T.; Yang, Y.; Shung, K.; et al. 3D printing of piezoelectric element for energy focusing and ultrasonic sensing. *Nano Energy* **2016**, *27*, 78–86. [CrossRef]
9. Cheng, J.; Chen, Y.; Wu, J.W.; Ji, X.R.; Wu, S.H. 3D Printing of $BaTiO_3$ Piezoelectric Ceramics for a Focused Ultrasonic Array. *Sensors* **2019**, *19*, 4078. [CrossRef] [PubMed]
10. Narita, F.; Fox, M. A Review on Piezoelectric, Magnetostrictive, and Magnetoelectric Materials and Device Technologies for Energy Harvesting Applications. *Adv. Eng. Mater.* **2018**, *20*, 1700743. [CrossRef]
11. Sakamoto, W.K.; Higuti, R.T.; Crivelini, E.B.; Nagashima, H.N. Polymer matrix-based piezoelectric composite for structural health monitoring. In Proceedings of the 2013 Joint IEEE International Symposium on Applications of Ferroelectric and Workshop on Piezoresponse Force Microscopy (ISAF/PFM), Prague, Czech Republic, 21–25 July 2013; pp. 295–297. [CrossRef]
12. Fang, X.; He, J.; Zhang, Y. Preparation and Characterization of Large-Area and Flexible Lead Zirconate Titanate/Polyvinyl-Butyral/Additives Composite Films for Piezoelectric Sensor Application. *Sens. Mater.* **2016**, *28*, 681–688. [CrossRef]
13. Pan, H.H.; Huang, M.W. Piezoelectric cement sensor-based electromechanical impedance technique for the strength monitoring of cement mortar. *Constr. Build. Mater.* **2020**, *254*, 119307. [CrossRef]
14. Sirohi, J.; Chopra, I. Fundamental Understanding of Piezoelectric Strain Sensors. *J. Intell. Mater. Syst. Struct.* **2000**, *11*, 246–257. [CrossRef]
15. Mitkus, R.; Pierou, A.; Feder, J.; Sinapius, M. Investigation and Attempt to 3D Print Piezoelectric 0-3 Composites Made of Photopolymer Resins and PZT. In Proceedings of the ASME 2020 Conference on Smart Materials, Adaptive Structures and Intelligent Systems, London, UK, 22–26 June 2020. [CrossRef]

16. Mitkus, R.; Taleb Alashkar, A.; Sinapius, M. An Attempt to Topology Optimize 3D Printed Piezoelectric Composite Sensors for Highest D31 Output. In Proceedings of the ASME 2021 Conference on Smart Materials, Adaptive Structures and Intelligent Systems, Virtual Conference, 14–15 September 2021. [CrossRef]
17. Pohl, J.; Willberg, C.; Gabbert, U.; Mook, G. Experimental and Theoretical Analysis of Lamb Wave Generation by Piezoceramic Actuators for Structural Health Monitoring. *Exp. Mech.* **2012**, *52*, 429–438. [CrossRef]
18. Raghavan, A.; Cesnik, C.E.S. Finite-dimensional piezoelectric transducer modeling for guided wave based structural health monitoring. *Smart Mater. Struct.* **2005**, *14*, 1448–1461. [CrossRef]